ACS Pharmacology & Translational Science

pubs.acs.org/ptsci Article

PARP Targeted Alpha-Particle Therapy Enhances Response to PD-1 Immune-Checkpoint Blockade in a Syngeneic Mouse Model of Glioblastoma

Hannah Dabagian, Tahereh Taghvaee, Paul Martorano, Daniel Martinez, Minu Samanta, Carolyn M. Watkins, Richard Chai, Adam Mansfield, Thomas J. Graham, John M. Maris, Daniel A. Pryma, Robert H. Mach, and Mehran Makvandi*

Cite This: *ACS Pharmacol. Transl. Sci.* 2021, 4, 344–351 Read Online

ACCESS | Metrics & More | Article Recommendations

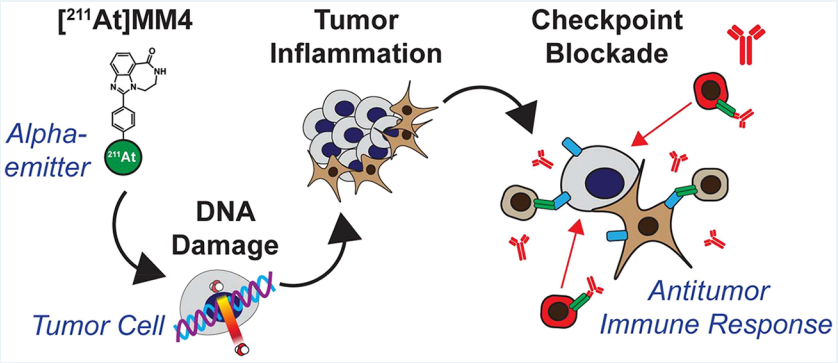

ABSTRACT: We have previously demonstrated potent antitumor effects of PARP targeted alpha-therapy with astatine-211-MM4 ([^{211}At]MM4) in neuroblastoma preclinical models, although differential sensitivity suggests it is unlikely to be curative as a single-agent in all tumor types. Alpha-particle induced DNA damage can elicit an immune response that results in T-cell activation against tumor cells; however, tumor cells can evade immune surveillance through expression of programmed death ligand 1 (PD-L1). Therefore, we investigated the effects of α particle therapy in combination with immune-checkpoint blockade using astatine-211-MM4 and anti-programmed death receptor 1 (anti-PD-1) immunotherapy in a syngeneic mouse model of glioblastoma. We characterized the sensitivity of four human glioblastoma cell lines to [^{211}At]MM4 *in vitro*. To evaluate [^{211}At]MM4 treatment effects on hematological tissues, complete blood counts were performed after a single dose at 12, 24, or 36 MBq/kg. In vivo efficacy was evaluated in a syngeneic mouse model of glioblastoma using GL26 glioblastoma cells in CB57BL/6J mice treated with either 36 MBq/kg [^{211}At]MM4, anti-PD-1 antibody, or a combination of the two. Following a single dose of [^{211}At]MM4, lymphocytes are significantly decreased compared to control at both 72 h and 1 week following treatment followed by recovery of counts by 2 weeks. However, neutrophils showed an increase with all dose levels of [^{211}At]MM4 exhibiting higher levels than control. The average best tumor responses for combination, anti-PD-1, and [^{211}At]MM4 were 100%, 83.6%, and 58.2% decrease in tumor volume, respectively. Average progression free intervals for combination, anti-PD-1, [^{211}At]MM4, and control groups was 65, 36.4, 23.2, and 3 days, respectively. The percentages of disease-free mice at the end of the study for combination and anti-PD-1 were 100% and 60%, while [^{211}At]MM4 and control groups were both 0%. In summary, combination therapy was more effective than either single agent in all response categories analyzed, highlighting the potential for PARP targeted alpha-therapy to enhance PD-1 immune-checkpoint blockade.

KEYWORDS: *astatine, radiopharmaceutical therapy, immune-checkpoint blockade, PD-1, PARP1, alpha-emitter, syngeneic, glioblastoma*

Alpha-particles can induce numerous double strand DNA breaks when traversing cell nuclei and are restricted to short ranges in tissue of <70 μm as a result of high-linear energy transfer properties.[1] Poly(ADP-ribose) polymerase 1 (PARP1) is abundantly expressed in cancer cell nuclei and can be used as a surrogate DNA target for alpha-particle therapy by conjugating astatine-211, a highly promising alpha-emitter, to

Received: December 2, 2020
Published: January 26, 2021

https://dx.doi.org/10.1021/acsptsci.0c00206
ACS Pharmacol. Transl. Sci. 2021, 4, 344–351

small molecule PARP inhibitors like astatine-211-MM4 ([^{211}At]MM4) reported herein.[2,3] This approach enables the pharmacological delivery of astatine-211 directly to cancer cell nuclei. Although PARP inhibitors are used clinically for the treatment of DNA repair deficient cancers and work through pharmacological inhibition or trapping of PARP1 on DNA which results in DNA damage, the mechanism of action of [^{211}At]MM4 is fundamentally different because DNA damage is induced by alpha-particle radiation independent of pharmacological mechanisms.[2] In addition, the biophysical properties of alpha-particles enable cellular lethality at concentrations over 1 billion times lower compared to chemical PARP inhibitors.[2] Furthermore, the DNA damage caused by PARP inhibitors is cell-cycle dependent only working in the s-phase during DNA replication, while alpha-particles induce DNA double strand breaks at all phases of the cell cycle, albeit with differential cellular lethality.[4−6] The enhanced lethality of alpha-particles to cells that progress through mitosis suggests that mitotic error is the primary mechanism of action for cellular lethality. Ionizing radiation has been shown to cause micronuclei formation which activates pattern recognition pathways to elicit an antitumor response.[7] This commonality between alpha-particle lethality to cells that progress through mitosis and the established role for micronuclei-pattern recognition led us to explore the immunogenicity of alpha-particles.

Immune-checkpoint blockade of inhibitory proteins expressed in the tumor microenvironment, such as programmed death ligand 1 (PD-L1), programmed death receptor 1 (PD-1), or cytotoxic T-lymphocyte protein 4 (CTLA-4), can unleash the immune system on tumor cells by blocking inhibitory signals. Interestingly, it has been shown that immune-checkpoint protein expression on host cells, specifically PD-L1, is required for maximum antitumor activity of anti-PD-1 or anti-PD-L1 therapy.[8] Immune-checkpoint blockade is one of the most promising strategies for cancer therapy; however, solid tumors remain largely unresponsive.[9] Current strategies focus on combinatorial therapy with DNA damaging agents that upregulate expression of immune-checkpoint proteins and prime the tumor by creating a proinflammatory state which is activatable by immune-checkpoint blockade.[9] The results from the MEDIOLA trial investigating anti-PDL1 therapy in combination with the DNA damaging agent olaparib showed promising antitumor activity with the combination in some patients; however, no difference was detected in progression free survival with olaparib monotherapy.[10] Previous work by our group showed that [^{211}At]MM4 has potent antitumor activity in preclinical models of neuroblastoma; however, other cancer types showed decreased sensitivity *in vitro*.[2] In addition, alpha-particles are highly cytotoxic to normal tissues, so exploring innovative approaches for harnessing the minimum effective dose through combinatorial therapy is highly desired. Therefore, in this study we explored utilizing [^{211}At]MM4 as an immunogenic stimulator in combination with an immune-checkpoint blockade anti-PD-1 inhibitor. By combining [^{211}At]MM4 with immune-checkpoint blockade we can selectively induce DNA damage and cell death in tumors to promote inflammation and enhance immunosurveillance in the tumor microenvironment. We evaluated the in vitro cytotoxicity of [^{211}At]MM4 in glioblastoma cell lines and performed preclinical studies investigating [^{211}At]MM4 and anti-PD-1 combination therapy in the GL26 syngeneic mouse model of glioblastoma. We used GL26 as a model system that can be broadly applied across multiple cancer types to test whether [^{211}At]MM4 can enhance the antitumor efficacy of immune-checkpoint blockade for "proof of concept".

MATERIALS AND METHODS

Cell Culture. Human glioblastoma (GBM) cell lines, U87MG, U87MG-IDH1 mutant, U118MG, and LN18, were cultured in RPMI growth media with 10% fetal bovine serum and 1% penicillin streptomycin. Cell lines were tested for mycoplasma at University of Pennsylvania Cell Center. Mouse GBM cell line GL26 was cultured in identical growth media as used for human GBM cell lines. All cell lines were purchased from ATCC except GL26 which was a kind gift from the Fan Lab at the University of Pennsylvania Department of Radiation Oncology.

[^{211}At]MM4 Synthesis. Astatine-211 was produced at the University of Pennsylvania Cyclotron Facility, and [^{211}At]MM4 was prepared through electrophilic aromatic destannylation of a tin precursor as previously described.[11] The final product was measured on a Capintec (Florham Park, NJ) dose calibrator and diluted to the desired concentration with saline.

***In Vitro* Cytotoxicity.** Cytotoxicity of [^{211}At]MM4 GBM cell lines was evaluated as previously described.[2] Briefly, cells were seeded at a density of 5000 cells/well in 96-well format 24 h before treatment with either [^{211}At]MM4 or nontargeted control [^{211}At]sodium astatide ([^{211}At]NaAt). Cells were treated with activities ranging from 1 kBq/mL to 1 MBq/mL, and cell viability was assessed 72 h post-treatment by using CellTiter Glo (Promega, Madison WI). The chemiluminescent signal was quantified on a Perkin-Elmer Enspire multimode plate reader (Waltham MA). Survival fraction was determined by normalizing the number of viable cells in vehicle control wells to the number of viable cells in treatment wells. Dose−response curves were generated using Prism GraphPad nonsigmoidal curve fitting, and the effective concentration for 50% reduction in viability (EC_{50}) was calculated. Experiments were performed in triplicate for each concentration and were repeated three times. PARP-1 expression was obtained from the Cancer Cell Line Encyclopedia at https://portals.broadinstitute.org/ccle/about#contact and analyzed to compare relative PARP1 mRNA expression between cell lines.

Animal Studies. All animal studies were performed under protocols approved by the University of Pennsylvania Institutional Animal Care and Use Committee (Philadelphia, PA).

***In Vivo* Hematological Toxicity.** Blood cells, predominately lymphocytes, are known to express high levels of PARP1; therefore, to assess hematological toxicities of [^{211}At]MM4, we performed complete blood count analysis at the time of euthanasia using a HEMAVET 950 FS blood analyzer (The Americas Drew Scientific Inc., Oxford CT). Female and male CB57BL/6J mice were treated with 12, 24, or 36 MBq/kg [^{211}At]MM4 and were euthanized at 4 weeks. In addition, we analyzed time-dependent effects at the 36 MBq/kg dose level and mice were euthanized at 72 h, 1 week, 2 week, and 4 week time points (n = 4 mice/treatment group except control and 36 MBq/kg n = 8 mice). At time of euthanasia, mice were anesthetized with mixed inhalation isoflurane/oxygen under a nose cone. Then terminal cardiac puncture was performed, and peripheral blood was transferred to K_2EDTA BD Microtainer tubes (BD, San Antonio, TX).

https://dx.doi.org/10.1021/acsptsci.0c00206
ACS Pharmacol. Transl. Sci. 2021, 4, 344−351

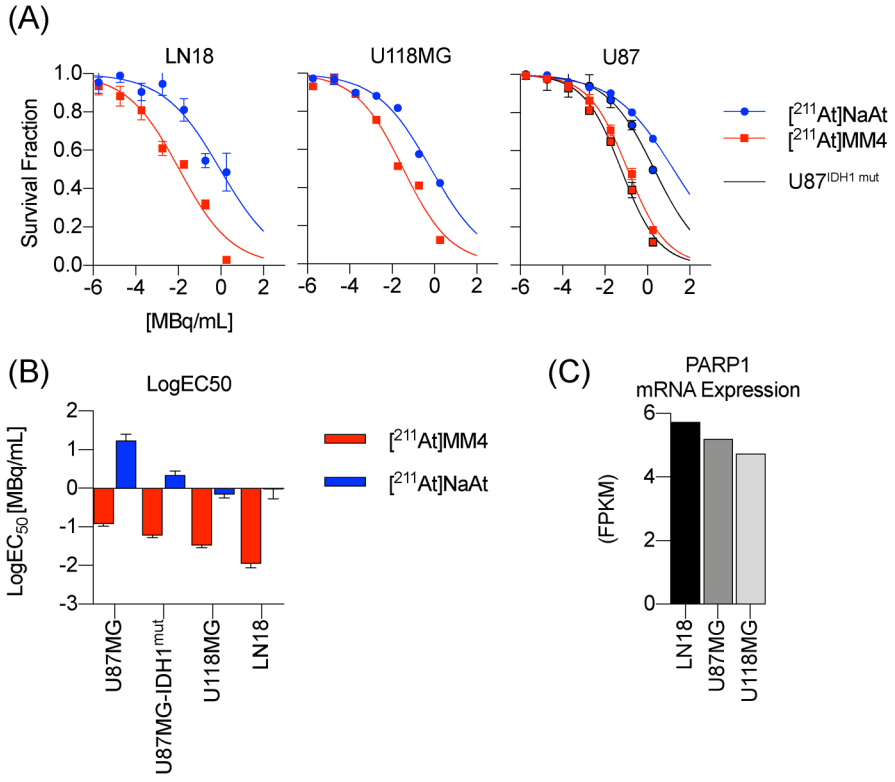

Figure 1. *In vitro* evaluation of [^{211}At]MM4 cytotoxicity in human glioblastoma (GBM) cell lines (experiments were performed in triplicate for each concentration and repeated three times). (A) Dose−response curves for each cell line or isogenic cell line pair treated with [^{211}At]MM4 or free astatine-211. (B) Bar graph of effective concentrations for 50% reduction in cell survival (EC_{50}) of treated GBM cell lines. (C) PARP1 mRNA expression in (GBM) cell lines obtained from the Cancer Cell Encyclopedia (https://portals.broadinstitute.org/ccle/about#contact) ([211At]NaAt: [211At] sodium astatide).

The sample volume injected on the HEMAVET 950 FS blood analyzer was 20 μL and was prespecified using the mouse protocol on the instrument. Lymphocyte and neutrophil blood counts were measured.

***In Vivo* Efficacy.** To evaluate therapeutic efficacy of alpha-particle therapy combined with immune checkpoint blockade, we used a syngeneic model of glioblastoma that was previously reported to show characteristic signs of immune evasion.[12,13] GL26 tumors were produced by subcutaneous injection of 1 million cells into the right flank in CB57BL/6J mice on day 0. Tumors were measured with a caliper, and tumor volume was calculated with the equation $((x/2)(y/2)(y/2))(4/3)$, where x is the largest dimension. There were four treatment arms (including saline control). Mice were treated with intraperitoneal injections of saline, 200 μg anti-PD1, 36 MBq/kg [^{211}At]MM4, or anti-PD1 in combination with [^{211}At]MM4 (n = 5/arm). Tumor bearing mice were enrolled once tumors were approximately 200 mm^3 into either a treatment group or control group on day 8, where day 0 is the day of tumor injections. Anti-PD1 was administered on days 8, 11, and 14. [^{211}At]MM4 was administered on day 11. Primary end points for efficacy were assessed by best tumor response (greatest reduction in tumor volume) and progression free interval (PFI is defined as the time from best response to a 25% increase in tumor volume). Secondary end points include complete response (no tumor regrowth after best response) and tumor growth rate modeled by nonlinear exponential growth. Mouse subject censorship was performed at the time of tumor progression or tumor stasis, to account for spontaneous remission of GL26 tumors as recommended by previous studies.[8]

Immunohistochemistry. After euthanasia, mouse tumors (n = 1/treatment group except [^{211}At]MM4 treatment group n = 2) were removed and fixed in 4% paraformaldehyde in PBS (Santa Cruz Biotechnology, Dallas, TX) for 24 h, transferred to PBS, paraffin-embedded, sectioned at 10 μm, and stained directly with HE (hematoxylin and eosin) as well as immunohistochemically using antibodies against PARP-1 [Clone 46C11], CD4 (Thermo 14-9766, 4SM95 clone), CD8 (mCD8a Dianova DIA-808, Clone GHH8), and F4/80 (Cell Signaling 70076, clone D259R) according to manufacturer protocols. Immunohistochemical staining was performed at the Children's Hospital of Philadelphia Pathology Core Laboratory. PARP-1 was used as a nonspecific tumor marker to assess [^{211}At]MM4 drug target expression. CD4 is a marker of helper T-cells and T-regulatory cells. We used CD4 as a biomarker to assess immunosurveillance in the tumor microenvironment. CD8 is a specific marker for cytotoxic T-cells (adaptive immune response), and F4/80 is a specific marker for macrophages (innate immune response). Tissue sections were analyzed by QuPath as previously described, and compared against control using percent difference in H-score and the number of positive cells detected categorized by intensity.[13]

Statistical Analysis. Prism 6 (GraphPad, La Jolla, CA) was used for all statistical analyses and data modeling. Dose−response curves were modeled using a nonlinear sigmoidal dose response to calculate the effective concentration for 50% cell survival (EC_{50}). Tumor growth curves were modeled using

https://dx.doi.org/10.1021/acsptsci.0c00206
ACS Pharmacol. Transl. Sci. 2021, 4, 344−351

a nonlinear exponential growth or decay to determine tumor growth rates. Hematological toxicity was evaluated by one-way ANOVA analysis with all treatment groups compared to control. Unless otherwise noted, all statistical testing was performed with significance denoted for p-values < 0.05 as tested by nonparametric unpaired t tests.

RESULTS

***In Vitro* Cytotoxicity.** [^{211}At]MM4 was more potent than unconjugated free astatine-211 in all cell lines evaluated (Figure 1A). Isogenic cell lines U87MG and U87MG-IDH1 mutant showed similar sensitivity, although the IDH1 mutant was more sensitive to both [^{211}At]MM4 and unconjugated free astatine-211. From dose−response curves, the effective dose for 50% reduction in survival was calculated and showed that the LN18 cell line is 10 times more sensitive than the U87MG cell line (Figure 1B). PARP1 mRNA expression obtained from the Cancer Cell Line Encyclopedia at https://portals.broadinstitute.org/ccle/about#contact was analyzed to assess if drug target expression was different between the cell lines, and we found that, despite LN18 showing over 10 times increased sensitivity, PARP1 mRNA was relatively equal (Figure 1C).

***In Vivo* Hematological Toxicity.** CBC analysis of CB57/Bl6 mice treated with escalating doses of [^{211}At]MM4 at the 4 week time point showed an increase in neutrophils in the 36 MBq/kg treatment group (p-value < 0.05 at 36 MBq/kg) (Figure 2A). A single dose of [^{211}At]MM4 at 36 MBq/kg caused a rapid decrease in lymphocytes at 3 and 7 day time points (one-way ANOVA analysis; p-value < 0.05) and partial recovery by 14 days, which showed reduced lymphocytes compared to control but differences were not statistically significant (Figure 2B). In contrast, neutrophils were elevated at the 4 week time points (one-way ANOVA analysis; p-value < 0.05), although mean differences were increased from control for all time points (Figure 2B). Data from 36 MBq/kg treatment and control group at 4 week time points were used in both analyses.

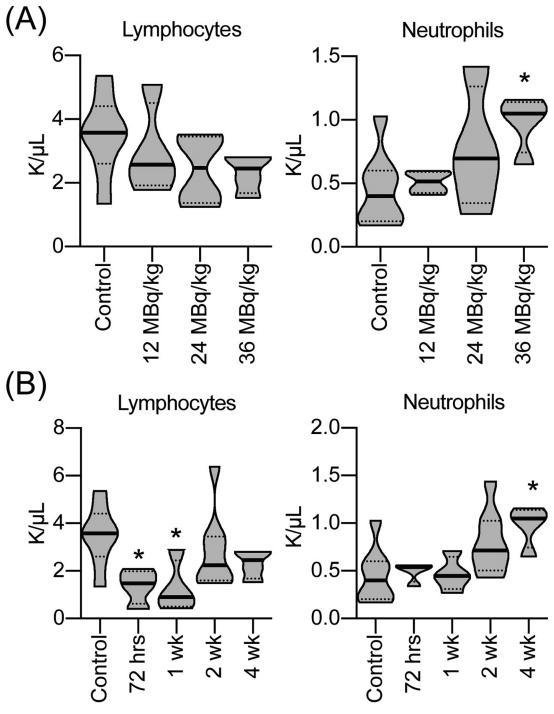

Figure 2. *In vivo* complete blood counts after treatment with (A) escalating doses of [^{211}At]MM4 4 weeks post-administration and (B) single dose of [^{211}At]MM4 at 36 MBq/kg evaluated at 3, 7, 14, and 28 day time points displayed as violin plots for white blood cell subpopulations, lymphocytes and neutrophils (n = 4/group except n = 8/group control and 36MBq/kg dose level; asterisk (*) denotes statistical significance by one-way ANOVA analysis; p-value < 0.05).

***In Vivo* Efficacy.** Combination therapy with [^{211}At]MM4 and anti-PD-1 was more effective than either single agent alone in nearly all efficacy measures analyzed. Individual tumor growth curves showed that single agent [^{211}At]MM4 was able to reduce tumor burden; however, all tumors eventually progressed following treatment (Figure 3A). Both anti-PD-1 and combination groups showed significant reduction in tumor burden (Figure 3A). The combination group showed the longest progression free interval (PFI) of 65 days (t test; p-value < 0.05) (Figure 3B) and best tumor response (t test; p-value < 0.05, except anti-PD-1 p-value = 0.0658) compared to all other groups (Figure 3C). Anti-PD-1 treated groups showed a longer PFI and greater tumor response compared to [^{211}At]MM4 (t test; p-value < 0.05). Despite longer PFI for the combination treated group, nonsignificant findings of best tumor response between combination and anti-PD1 treated groups were supported in favor of combination therapy by analyzing the percentage of complete responses in each group (Figure 3D). In addition, the rate of tumor growth was slowest, which equaled a faster tumor response, in the combination group compared to [^{211}At]MM4 (t test; p-value < 0.05). No significant differences in tumor growth rates were found between combination and anti-PD-1 or [^{211}At]MM4 and anti-PD-1 treatment groups (Figure 3E). All tumors were relatively similar in size at the start of the study (Figure 3F). Together these data provide evidence to support that combination treatment with [^{211}At]MM4 and anti-PD-1 is more effective than treatment with either agent alone.

Immunohistochemistry. No tumors from combination groups were available for histopathology analyses. The control GL26 tumor showed a relatively healthy tumor microenvironments with large tumor cell burden (n = 1). Remarkable host immune cell and tumor interactions can be noted in the HE staining of anti-PD-1 treated tumor (n = 1) (Figure 4A). Clear images of immune cells entering the tumor microenvironment creating nodules with PARP1 positive tumor cells undergoing apoptosis can be seen. The anti-PD-1 treated tumor showed enhanced tumor infiltration of CD4$^+$ T-cells and CD8$^+$ cytotoxic T-cells (Figure 4A), while the tumor from a good responder from the [^{211}At]MM4 treatment group showed a stark difference in number of tumor-associated macrophages compared to all other groups and increased CD4$^+$ T-cells compared to control (n = 1) (Figure 4A). In comparison, a poor responder from the [^{211}At]MM4 treatment group showed few CD4$^+$ T-cells and fewer macrophages, similar to control (Figure 4A). Quantification of tumor sections for cell number and intensity/area showed [^{211}At]MM4 (good responder only) had increased macrophages and CD4$^+$ T-cells, but decreased CD8$^+$ T-cells compared to control (Figure 4B). The anti-PD-1 showed increases in CD4$^+$/CD8$^+$ and macrophages compared to control. Both the [^{211}At]MM4 good responder and anti-PD-1 treated tumors showed decreased PARP1 positive cells which indicates decreasing tumor burden. However, a higher number of +3 intensity for PARP1 staining was observed in the [^{211}At]MM4 good responder tumor section (Figure 4C). In

https://dx.doi.org/10.1021/acsptsci.0c00206
ACS Pharmacol. Transl. Sci. 2021, 4, 344−351

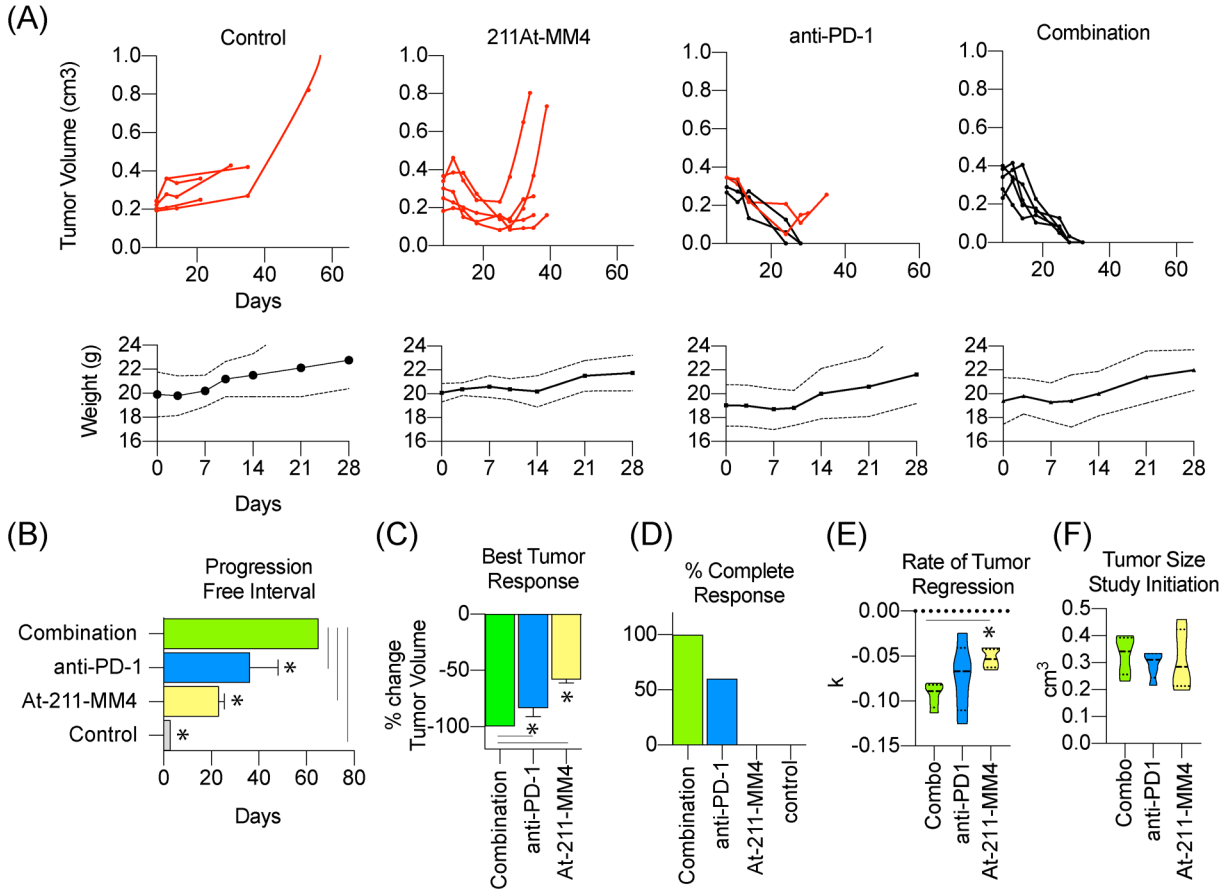

Figure 3. *In vivo* efficacy analysis of single-agent or combination therapy using [^{211}At]MM4 and/or anti-PD-1 (n = 5/group). Mouse weights are shown below for each treatment arm (dotted lines represent standard error bands). (A) Individual tumor growth curves for control, single-agent, and combination treated groups. Red lines signify mouse subjects that progressed after best response. (B) Swimmer plot of average progression free interval of each group. (C) Waterfall plot of best tumor response after treatment. (D) Bar graph showing percentage of complete responses for each treatment group. (E,F) Violin plots for (E) tumor growth rate (k) modeled for each treatment group and (F) tumor size at initiation of study.

general, the largest differences in the number of positive cells compared to control were observed at the + 3 staining intensity for all biomarkers.

DISCUSSION

The use of immune-checkpoint blockade has transformed how we treat cancer, and it is now widely recognized that even chemotherapy likely has a proinflammatory role for eliciting a response.[9] DNA damage has been shown to activate the immune response in glioblastoma GL261 orthotopic tumor models through stimulator of interferon genes (STING) mediated pathways that activate phagocytic activity of macrophages and initiate the innate to adaptive transfer of immunity.[14] The authors demonstrated that anti-CD47 therapy is not sufficient to promote phagocytic activity of macrophages; however, when combined with DNA alkylating agent temozolomide or DNA cross-linking agent cisplatin, phagocytic activity was enhanced and resulted in antitumor effects.[14] Interestingly, this antitumor response by the innate immune system was shown to activate the immune checkpoint, and sequential anti-PD-1 therapy increased antitumor responses, producing complete responses in 40% of treated mice.[14] As a cytosolic sensor, STING recognizes cytoplasmic DNA, viral, or bacterial molecules and then releases biochemical signals to alert nearby cells or neighboring tissue of an active infection which mediates the recruitment of immune cells. The antiviral response can also be activated by host cell DNA that enters the cytoplasm as a result of mitotic error-micronuclei formation.[7] Since we know alpha-particles cause immense levels of double strand DNA breaks and are most lethal to cells in mitosis, we propose that alpha-particles likely have the ability to stimulate pattern recognition pathways. Although this was not confirmed in our study, it has been shown in GL261 tumor models which are a clonal relative to the GL26 tumor model reported here. The purpose of the present study was to investigate whether PARP targeted alpha-particles can enhance the immunogenicity of tumors to improve the efficacy of checkpoint-blockade inhibitors.

In vitro, we observed direct cytotoxic effects of PARP targeted alpha particles by comparing [^{211}At]MM4 to unconjugated free astatine-211. Due to the short-range of alpha-particles in biological mediums like water, the unconjugated free astatine-211 has a lower probability of decaying within the 70 μm range required to hit target cells with alpha-particles. With the pharmacological delivery of astatine-211 directly to cancer chromatin, via [^{211}At]MM4 binding to PARP1, there is a higher probability of alpha-particles traversing the nucleus and this is likely the reason why [^{211}At]MM4 is 50−100 times more cytotoxic than free astatine-211. These data further support [^{211}At]MM4 as having direct toxicity though DNA damage as previously reported.[2]

https://dx.doi.org/10.1021/acsptsci.0c00206
ACS Pharmacol. Transl. Sci. 2021, 4, 344−351

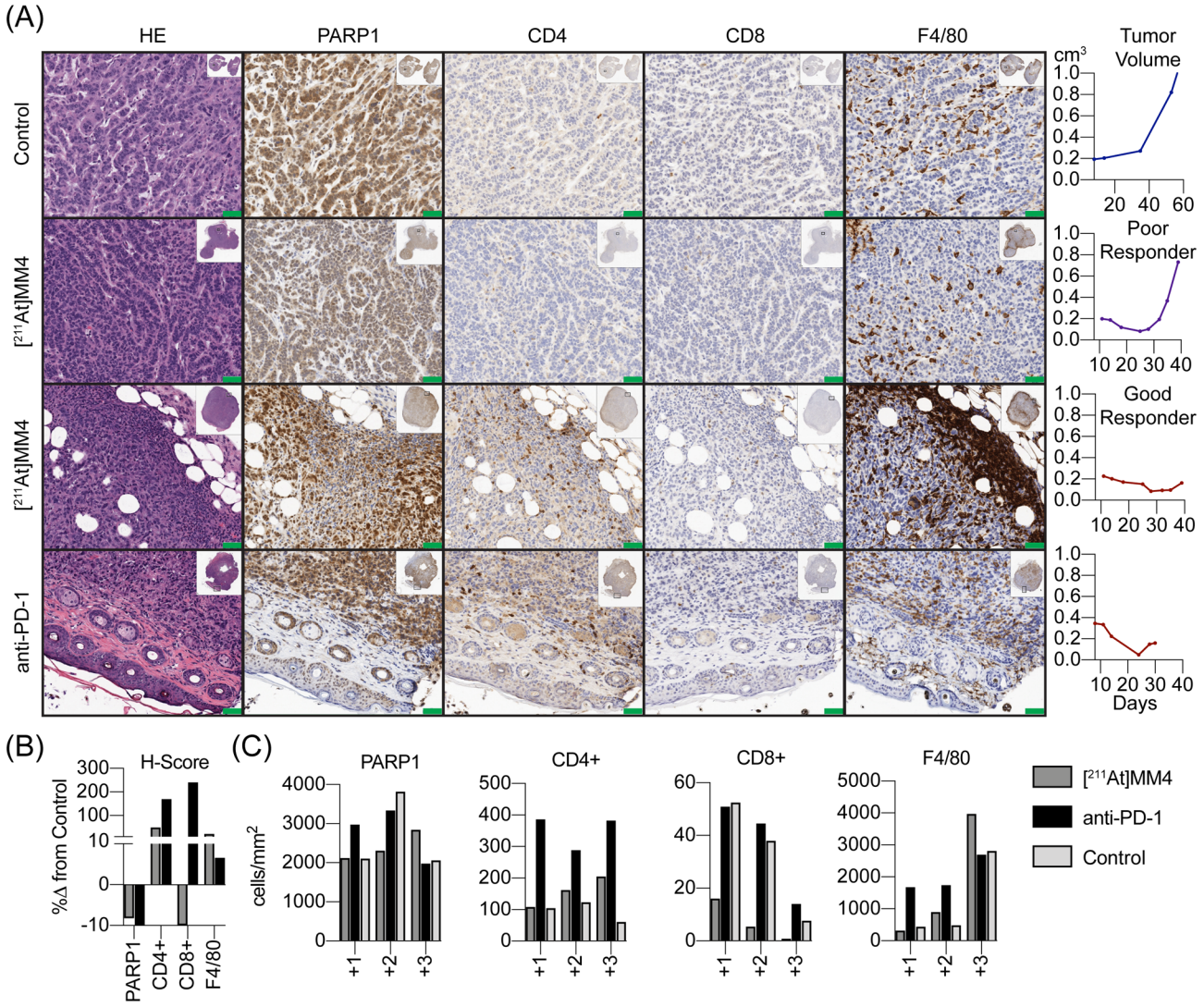

Figure 4. (A) Tumor tissue histology of control (n = 1), [^{211}At]MM4 poor responder (n = 1), [^{211}At]MM4 good responder (n = 1), and anti-PD-1 treated tumors stained by hematoxylin and eosin (HE) for gross pathology, PARP1, CD4, CD8, and F4/80 biomarkers. Scale bars = 50 μm. (B) Quantification of biomarkers using percent difference in H-score from control and (C) number of cells detected classified by intensity for tumor sections from control (n = 1), [^{211}At]MM4 good responder (n = 1), and anti-PD-1 treated tumors (n = 1).

By assessing the in vivo hematological toxicity of [^{211}At]-MM4, we gained further insight into how this treatment may affect the tumor microenvironment, particularly immune cells. PARP1 expression is highest in lymphocytes > macrophages > neutrophils. In agreement, we showed [^{211}At]MM4 is cytotoxic to normal mouse lymphocytes at 36 MBq/kg, although lymphocyte counts recover by 2 weeks. No toxicity was observed to neutrophils; instead treated mice exhibited dose dependent increases which resemble the clinical sign of infection or inflammation. The fact that the [^{211}At]MM4 treated tumor from a good responder resulted in strong macrophage recruitment and that this was not seen in poor responders that had fast progressing tumors after the time of best response, suggests that [^{211}At]MM4 triggers tumor inflammation but may also kill important tumor associated-lymphocytes that are required for the innate-to-adaptive immunity transfer. This proposed mechanism of [^{211}At]MM4 depletion of T-cells is confounded by the recovery of circulating lymphocytes by 2 weeks post-treatment, an event that precedes the time for tumor progression. Instead, the more likely scenario is that after the inflammatory effects of [^{211}At]MM4 subside, tumor associated macrophages become polarized to anti-inflammatory phenotypes. This is an established property of tumor associated macrophages which express immune-checkpoint proteins including PD-L1 and PD-1.[15−17] This concept is further supported by previous work that showed PD-1 expression increases after DNA damage in GL261 tumors, especially in the poor responders.[14] We did not test for PD-1 expression in tumors; however, our data showed that addition of anti-PD-1 therapy to [^{211}At]MM4 produced 100% response rates in GL26 tumors which strengthens this conclusion.

A recent study demonstrated that PD-1 binding on T-cells to PD-L1 on tumor-associated macrophages inhibits T-cell activation and was negatively correlated with response to immune-checkpoint blockade.[13] Interestingly, tumor associated macrophages with high PD-L1 expression showed reduced phagocytic properties and anti-PD-L1 treatment did not restore antitumor phagocytosis.[13] In the present study, we saw direct evidence of macrophage phagocytic activity in a [^{211}At]MM4 treated tumor assessed by histopathology, which suggested proinflammatory signaling mediated by [^{211}At]MM4

https://dx.doi.org/10.1021/acsptsci.0c00206
ACS Pharmacol. Transl. Sci. 2021, 4, 344−351

activated macrophages. Furthermore, we found enhanced immunosurveillance in this tumor displayed by exceedingly high levels of $CD4^+$ T-cells. The presence of $CD4^+$ T-cells was highest in the anti-PD-1 treated tumor. Although $CD4^+$ T-cells can have direct antitumor activity, they can also become T-regulatory cells that allow immune escape. In our study, we observed a higher number of $CD4^+$ T-cells in tumors that were responsive to therapy which suggests antitumor activity, although this response was not sufficient to completely eradicate the tumor burden.

A limitation of the present study includes the lack of biochemical analyses to further validate mechanisms by which alpha-particles stimulate tumor associated inflammation. In particular, we did not perform histopathological analysis on tumors from the combination treatment group due to the unavailability of tumors as a result from complete responses. Future studies are being designed to account for these factors and will be directed to analyzing the effects on the tumor microenvironment. One difficulty with interpreting the results from syngeneic tumor models is the high propensity for tumors to spontaneously resolve due to antitumor immunity.[8] To account for this, we employed multiple measures of efficacy and censored mice at early signs of progression. Immunohistochemical staining showed anti-PD-1 treated tumors did have tumor cell burden remaining at the time of censorship, although there was a direct sign of antitumor immunity including the $CD8^+$ T-cells and macrophage infiltration. This confounding result however is balanced by the expedient complete remissions observed in the combination group, suggesting there is direct efficacy enhancement of immune checkpoint-blockade with [^{211}At]MM4.

We propose that [^{211}At]MM4 stimulates tumor inflammation through direct DNA damage to tumor cells which activates the innate immune response. We know astatine-211 is not equally toxic to different cell types (tumor or host) and toxicity is dependent on microscopic distribution relative to cell nuclei. PARP1 IHC showed that tumor cells were more positive than stromal or immune cells, which highlights that delivered alpha-particles are selectively irradiating tumor cells. This proposed mechanism is supported by the increase in circulating neutrophils as a nonspecific inflammatory marker that is often a hallmark sign of the antiviral innate immune response. These data are not sufficient to confirm STING pattern recognition pathway activation in the tumor microenvironment, although other reports have robustly demonstrated this and support pattern recognition as a plausible explanation for [^{211}At]MM4 mediated inflammation. The enhanced recruitment of macrophages to tumors treated with [^{211}At]MM4 further supports the proposed mechanism, although the exact role of macrophages for mediating antitumor immunity is unclear. Nevertheless, it is a sign of tumor inflammation. These observations combined with more rapid complete responses observed in the combination treated group compared to the anti-PD-1 treated group suggest there is a beneficial role of macrophage recruitment. In summary, these data show that PARP targeted alpha-particles from [^{211}At]MM4 can recruit immune cells which may provide a rationale for the observed improvement in antitumor efficacy when combined with anti-PD-1 checkpoint blockade.

AUTHOR INFORMATION

Corresponding Author

Mehran Makvandi − *Division of Nuclear Medicine and Clinical Molecular Imaging, Department of Radiology, University of Pennsylvania Perelman School of Medicine, Philadelphia, Pennsylvania 19104, United States;* orcid.org/0000-0002-6315-4942; Email: makvandi@pennmedicine.upenn.edu

Authors

Hannah Dabagian − *Division of Nuclear Medicine and Clinical Molecular Imaging, Department of Radiology, University of Pennsylvania Perelman School of Medicine, Philadelphia, Pennsylvania 19104, United States*

Tahereh Taghvaee − *Division of Nuclear Medicine and Clinical Molecular Imaging, Department of Radiology, University of Pennsylvania Perelman School of Medicine, Philadelphia, Pennsylvania 19104, United States*

Paul Martorano − *Division of Nuclear Medicine and Clinical Molecular Imaging, Department of Radiology, University of Pennsylvania Perelman School of Medicine, Philadelphia, Pennsylvania 19104, United States*

Daniel Martinez − *Department of Pathology, Children's Hospital of Philadelphia, Philadelphia, Pennsylvania 19104, United States*

Minu Samanta − *Division of Oncology and Center for Childhood Cancer Research, Children's Hospital of Philadelphia, Philadelphia, Pennsylvania 19104, United States; Department of Pediatrics, Perelman School of Medicine at the University of Pennsylvania, Philadelphia, Pennsylvania 19104, United States*

Carolyn M. Watkins − *Division of Nuclear Medicine and Clinical Molecular Imaging, Department of Radiology, University of Pennsylvania Perelman School of Medicine, Philadelphia, Pennsylvania 19104, United States*

Richard Chai − *Division of Nuclear Medicine and Clinical Molecular Imaging, Department of Radiology, University of Pennsylvania Perelman School of Medicine, Philadelphia, Pennsylvania 19104, United States*

Adam Mansfield − *Division of Nuclear Medicine and Clinical Molecular Imaging, Department of Radiology, University of Pennsylvania Perelman School of Medicine, Philadelphia, Pennsylvania 19104, United States*

Thomas J. Graham − *Division of Nuclear Medicine and Clinical Molecular Imaging, Department of Radiology, University of Pennsylvania Perelman School of Medicine, Philadelphia, Pennsylvania 19104, United States*

John M. Maris − *Division of Oncology and Center for Childhood Cancer Research, Children's Hospital of Philadelphia, Philadelphia, Pennsylvania 19104, United States*

Daniel A. Pryma − *Division of Oncology and Center for Childhood Cancer Research, Children's Hospital of Philadelphia, Philadelphia, Pennsylvania 19104, United States; Department of Pediatrics, Perelman School of Medicine at the University of Pennsylvania, Philadelphia, Pennsylvania 19104, United States*

Robert H. Mach − *Division of Nuclear Medicine and Clinical Molecular Imaging, Department of Radiology, University of Pennsylvania Perelman School of Medicine, Philadelphia, Pennsylvania 19104, United States;* orcid.org/0000-0002-7645-2869

Complete contact information is available at:

https://dx.doi.org/10.1021/acsptsci.0c00206
ACS Pharmacol. Transl. Sci. 2021, 4, 344−351

https://pubs.acs.org/10.1021/acsptsci.0c00206

Author Contributions

The manuscript was written through contributions of all authors. All authors have given approval to the final version of the manuscript.

Funding

This work was supported by the Pearl and Phillip Basser Innovation Research Award (to M.M.), the McCabe Foundation Fellow Scholar Award (M.M.), the NIH and NCI (1R01CA219006-01A1, to D.A.P., and R35 CA220500, to J.M.M.). The production of astatine-211 used in this proposal was supported by the Bromine and Astatine isotope production and research development grant funded by the Department of Energy Nuclear Physics Isotope Program (DE-SC0017646, to R H.M.).

Notes

The authors declare the following competing financial interest(s): R.H.M., D.A.P., and M.M. are inventor and co-inventors on a pending patent for a 211At-PARP targeted radiotherapy. All other authors declare that the research was conducted in the absence of any commercial or financial relationships that could be construed as a potential conflict of interest.

REFERENCES

(1) Sgouros, G., Roeske, J. C., McDevitt, M. R., Palm, S., Allen, B. J., Fisher, D. R., Brill, A. B., Song, H., Howell, R. W., Akabani, G., Committee, S. M., Bolch, W. E., Brill, A. B., Fisher, D. R., Howell, R. W., Meredith, R. F., Sgouros, G., Wessels, B. W., and Zanzonico, P. B. (2010) MIRD Pamphlet No. 22 (abridged): radiobiology and dosimetry of alpha-particle emitters for targeted radionuclide therapy. *J. Nucl. Med. 51* (2), 311−28.

(2) Makvandi, M., Lee, H., Puentes, L. N., Reilly, S. W., Rathi, K. S., Weng, C. C., Chan, H. S., Hou, C., Raman, P., Martinez, D., Xu, K., Carlin, S. D., Greenberg, R. A., Pawel, B. R., Mach, R. H., Maris, J. M., and Pryma, D. A. (2019) Targeting PARP-1 with Alpha-Particles Is Potently Cytotoxic to Human Neuroblastoma in Preclinical Models. *Mol. Cancer Ther. 18* (7), 1195−1204.

(3) Lee, H., Riad, A., Martorano, P., Mansfield, A., Samanta, M., Batra, V., Mach, R. H., Maris, J. M., Pryma, D. A., and Makvandi, M. (2020) PARP-1-Targeted Auger Emitters Display High-LET Cytotoxic Properties In Vitro but Show Limited Therapeutic Utility in Solid Tumor Models of Human Neuroblastoma. *J. Nucl. Med. 61* (6), 850−856.

(4) Bird, R. P., Rohrig, N., Colvett, R. D., Geard, C. R., and Marino, S. A. (1980) Inactivation of synchronized Chinese Hamster V79 cells with charged-particle track segments. *Radiat. Res. 82* (2), 277−89.

(5) Lyckesvard, M. N., Delle, U., Kahu, H., Lindegren, S., Jensen, H., Back, T., Swanpalmer, J., and Elmroth, K. (2014) Alpha particle induced DNA damage and repair in normal cultured thyrocytes of different proliferation status. *Mutat. Res., Fundam. Mol. Mech. Mutagen. 765*, 48−56.

(6) Claesson, K., Magnander, K., Kahu, H., Lindegren, S., Hultborn, R., and Elmroth, K. (2011) RBE of alpha-particles from (211)At for complex DNA damage and cell survival in relation to cell cycle position. *Int. J. Radiat. Biol. 87* (4), 372−84.

(7) Harding, S. M., Benci, J. L., Irianto, J., Discher, D. E., Minn, A. J., and Greenberg, R. A. (2017) Mitotic progression following DNA damage enables pattern recognition within micronuclei. *Nature 548* (7668), 466−470.

(8) Lau, J., Cheung, J., Navarro, A., Lianoglou, S., Haley, B., Totpal, K., Sanders, L., Koeppen, H., Caplazi, P., McBride, J., Chiu, H., Hong, R., Grogan, J., Javinal, V., Yauch, R., Irving, B., Belvin, M., Mellman, I., Kim, J. M., and Schmidt, M. (2017) Tumour and host cell PD-L1 is required to mediate suppression of anti-tumour immunity in mice. *Nat. Commun. 8*, 14572.

(9) Galluzzi, L., Humeau, J., Buque, A., Zitvogel, L., and Kroemer, G. (2020) Immunostimulation with chemotherapy in the era of immune checkpoint inhibitors. *Nat. Rev. Clin. Oncol. 17*, 725.

(10) Domchek, S. M., Postel-Vinay, S., Im, S. A., Park, Y. H., Delord, J. P., Italiano, A., Alexandre, J., You, B., Bastian, S., Krebs, M. G., Wang, D., Waqar, S. N., Lanasa, M., Rhee, J., Gao, H., Rocher-Ros, V., Jones, E. V., Gulati, S., Coenen-Stass, A., Kozarewa, I., Lai, Z., Angell, H. K., Opincar, L., Herbolsheimer, P., and Kaufman, B. (2020) Olaparib and durvalumab in patients with germline BRCA-mutated metastatic breast cancer (MEDIOLA): an open-label, multicentre, phase 1/2, basket study. *Lancet Oncol. 21* (9), 1155−1164.

(11) Reilly, S. W., Makvandi, M., Xu, K., and Mach, R. H. (2018) Rapid Cu-Catalyzed [(211)At]Astatination and [(125)I]Iodination of Boronic Esters at Room Temperature. *Org. Lett. 20* (7), 1752−1755.

(12) Oh, T., Fakurnejad, S., Sayegh, E. T., Clark, A. J., Ivan, M. E., Sun, M. Z., Safaee, M., Bloch, O., James, C. D., and Parsa, A. T. (2014) Immunocompetent murine models for the study of glioblastoma immunotherapy. *J. Transl. Med. 12*, 107.

(13) Aslan, K., Turco, V., Blobner, J., Sonner, J. K., Liuzzi, A. R., Nunez, N. G., De Feo, D., Kickingereder, P., Fischer, M., Green, E., Sadik, A., Friedrich, M., Sanghvi, K., Kilian, M., Cichon, F., Wolf, L., Jahne, K., von Landenberg, A., Bunse, L., Sahm, F., Schrimpf, D., Meyer, J., Alexander, A., Brugnara, G., Roth, R., Pfleiderer, K., Niesler, B., von Deimling, A., Opitz, C., Breckwoldt, M. O., Heiland, S., Bendszus, M., Wick, W., Becher, B., and Platten, M. (2020) Heterogeneity of response to immune checkpoint blockade in hypermutated experimental gliomas. *Nat. Commun. 11* (1), 931.

(14) von Roemeling, C. A., Wang, Y., Qie, Y., Yuan, H., Zhao, H., Liu, X., Yang, Z., Yang, M., Deng, W., Bruno, K. A., Chan, C. K., Lee, A. S., Rosenfeld, S. S., Yun, K., Johnson, A. J., Mitchell, D. A., Jiang, W., and Kim, B. Y. S. (2020) Therapeutic modulation of phagocytosis in glioblastoma can activate both innate and adaptive antitumour immunity. *Nat. Commun. 11* (1), 1508.

(15) Patel, S. J., Sanjana, N. E., Kishton, R. J., Eidizadeh, A., Vodnala, S. K., Cam, M., Gartner, J. J., Jia, L., Steinberg, S. M., Yamamoto, T. N., Merchant, A. S., Mehta, G. U., Chichura, A., Shalem, O., Tran, E., Eil, R., Sukumar, M., Guijarro, E. P., Day, C. P., Robbins, P., Feldman, S., Merlino, G., Zhang, F., and Restifo, N. P. (2017) Identification of essential genes for cancer immunotherapy. *Nature 548* (7669), 537−542.

(16) Gabrusiewicz, K., Li, X., Wei, J., Hashimoto, Y., Marisetty, A. L., Ott, M., Wang, F., Hawke, D., Yu, J., Healy, L. M., Hossain, A., Akers, J. C., Maiti, S. N., Yamashita, S., Shimizu, Y., Dunner, K., Zal, M. A., Burks, J. K., Gumin, J., Nwajei, F., Rezavanian, A., Zhou, S., Rao, G., Sawaya, R., Fuller, G. N., Huse, J. T., Antel, J. P., Li, S., Cooper, L., Sulman, E. P., Chen, C., Geula, C., Kalluri, R., Zal, T., and Heimberger, A. B. (2018) Glioblastoma stem cell-derived exosomes induce M2 macrophages and PD-L1 expression on human monocytes. *Oncoimmunology 7* (4), e1412909.

(17) Lamano, J. B., Lamano, J. B., Li, Y. D., DiDomenico, J. D., Choy, W., Veliceasa, D., Oyon, D. E., Fakurnejad, S., Ampie, L., Kesavabhotla, K., Kaur, R., Kaur, G., Biyashev, D., Unruh, D. J., Horbinski, C. M., James, C. D., Parsa, A. T., and Bloch, O. (2019) Glioblastoma-Derived IL6 Induces Immunosuppressive Peripheral Myeloid Cell PD-L1 and Promotes Tumor Growth. *Clin. Cancer Res. 25* (12), 3643−3657.